Cooperative macromolecular device revealed by meta-analysis of static and time-resolved structures

Zhong Ren[a,1], Vukica Šrajer[a], James E. Knapp[b], and William E. Royer, Jr.[c]

[a]Center for Advanced Radiation Sources, University of Chicago, 9700 South Cass Avenue, Building 434B, Argonne, IL 60439; [b]Department of Biomedical Sciences, Mercer University School of Medicine, Savannah, GA 31404; and [c]Department of Biochemistry and Molecular Pharmacology, University of Massachusetts Medical School, Worcester, MA 01655

Edited by Charles L. Brooks III, University of Michigan, Ann Arbor, MI, and accepted by the Editorial Board October 18, 2011 (received for review June 09, 2011)

Here we present a meta-analysis of a large collection of static structures of a protein in the Protein Data Bank in order to extract the progression of structural events during protein function. We apply this strategy to the homodimeric hemoglobin HbI from *Scapharca inaequivalvis*. We derive a simple dynamic model describing how binding of the first ligand in one of the two chemically identical subunits facilitates a second binding event in the other partner subunit. The results of our ultrafast time-resolved crystallographic studies support this model. We demonstrate that HbI functions like a homodimeric mechanical device, such as pliers or scissors. Ligand-induced motion originating in one subunit is transmitted to the other via conserved pivot points, where the E and F′ helices from two partner subunits are "bolted" together to form a stable dimer interface permitting slight relative rotation but preventing sliding.

allostery | cooperativity | structural dynamics | time-resolved crystallography

Hemoglobins are molecular oxygen transporters in vertebrates and many invertebrates. Although the variety of quaternary assemblies of hemoglobins (1, 2) suggests considerable diversity in the strategies to achieve cooperativity, a general hypothesis remains valid: A newly ligated subunit communicates with its unligated partners via conformational changes, either tertiary or quaternary, thereby altering the ligand affinity of its partner subunits (3–5). However, the key question remains obscure: How are ligand-induced structural changes that originate in one subunit transmitted to the other to structurally modulate its ligand binding affinity? This paper harnesses structural evidence presently embedded in a large number of static and time-resolved structures of HbI and presents a simple cooperative mechanism. We take advantage of noncrystallographic symmetry (NCS) as a unique opportunity to examine asymmetric, but cooperative, behavior between subunits in different structural environments imposed by crystal lattices (6) (Fig. S1). The main finding of this study is summarized by an animated cartoon (Movie S1) showing our proposed cooperative mechanical model in action.

Unlike mammalian hemoglobins, the interface of HbI homodimer consists of a longer and straight helix E and a bent helix F from each subunit (1, 7). These two helices hold a heme group in between (Figs. 1*A* and 2*A*). Each heme group is anchored to the proximal His101 located near the end of helix F. In this paper, we refer to the two subunits as A and B and the two helices in one subunit as E and F. The notations E′ and F′ refer to E and F in the partner subunit.

Results

Here we propose a simple mechanical model to explain the mechanism of cooperative change in ligand binding affinity in homodimeric HbI (Fig. 1*A* and Movies S1 and S2). In this model, motions transmit from one subunit to the other via two pairs of "bolted" helices E–F′ and E′–F at the dimer interface so that the majority of the intersubunit contacts remain undisturbed during transition between allosteric states (Fig. 1*A*). Starting from a structure with two fully ligated subunits, this mechanical device models a cascade of structural events triggered by ligand dissociation at only one of the two heme sites (top blue heme in Fig. 1*A* and heme B in crystal lattices). F′ is pushed away from E′ by the out-of-heme-plane motion of Fe and the associated proximal His101′ displacement. A helix bending hinge near the middle of E′ (Figs. 1*A* and 2) permits the C-terminal half of E′ to move together with F′ as an integral rigid body. Because E is tightly jointed to F′ across the dimer interface in the bolt region via Gly68 at the position E6 (Fig. 1 *A* and *B*), the N-terminal half of E also moves along with F′, consequently increasing the E–F angle in the red subunit. E contains the distal His69 at the position E7 next to Gly68 (Fig. 1*B*) such that movement of E directly impacts ligand affinity by lengthening and weakening the hydrogen bond between the ligand and the distal histidine, thus promoting the second ligand dissociation. As a result of these concerted motions, the right half of the dimer interface rotates clockwise around the bending hinges of E and E′ near their crossing point (Fig. 1*A*). With both ligands dissociated, the overall motions of this proposed mechanical device fully account for the quaternary rotation of HbI previously observed (7, 8).

We provide four lines of evidence to support this cooperative model. (*i*) Our meta-analysis applied to all HbI structures in Protein Data Bank (PDB) reveals that the space between E and F increases upon ligand dissociation, resulting in a more open heme pocket in its unligated state. This model critically relies on the correlation between ligand binding affinity and heme pocket conformation. (*ii*) We observe that the hinge of the E–F motion is located at the middle of E rather than the EF corner. It is obvious from the cartoon in Fig. 1*A* that the E–F angle would not increase in the red subunit, if the hinge were at the EF corner. (*iii*) We note that several conserved residues form the E–F′ junction as if these helices are bolted together to allow slight rotation but not relative sliding. It is conceivable that without such tight intersubunit engagement, backlash would prevent motion from being transmitted. (*iv*) In addition, we obtain direct observations from time-resolved experiments of asymmetrically ligated structures that mimic a singly ligated state, depicting this mechanical device at the midpoint of operation and stopped at an intermediate step.

(*i*) By superposition of all HbI structures in PDB (Figs. 2 *C*–*E*), we identify that the ligand-induced clamshell motion between E and F is significant and systematic in HbI. E and F motions have

Author contributions: Z.R. designed research; Z.R., V.Š., and W.E.R. performed research; Z.R., J.E.K., and W.E.R. contributed new reagents/analytic tools; Z.R. and V.Š. analyzed data; and Z.R. wrote the paper.

The authors declare no conflict of interest.

This article is a PNAS Direct Submission. C.L.B. is a guest editor invited by the Editorial Board.

Freely available online through the PNAS open access option.

Data deposition: Atomic coordinates and structure factors for the reported crystal structure at 100 ps have been deposited in the Protein Data Bank, www.pdb.org (PDB ID code 3QOB).

[1]To whom correspondence should be addressed. E-mail: renz@uchicago.edu.

This article contains supporting information online at www.pnas.org/lookup/suppl/doi:10.1073/pnas.1109213108/-/DCSupplemental.

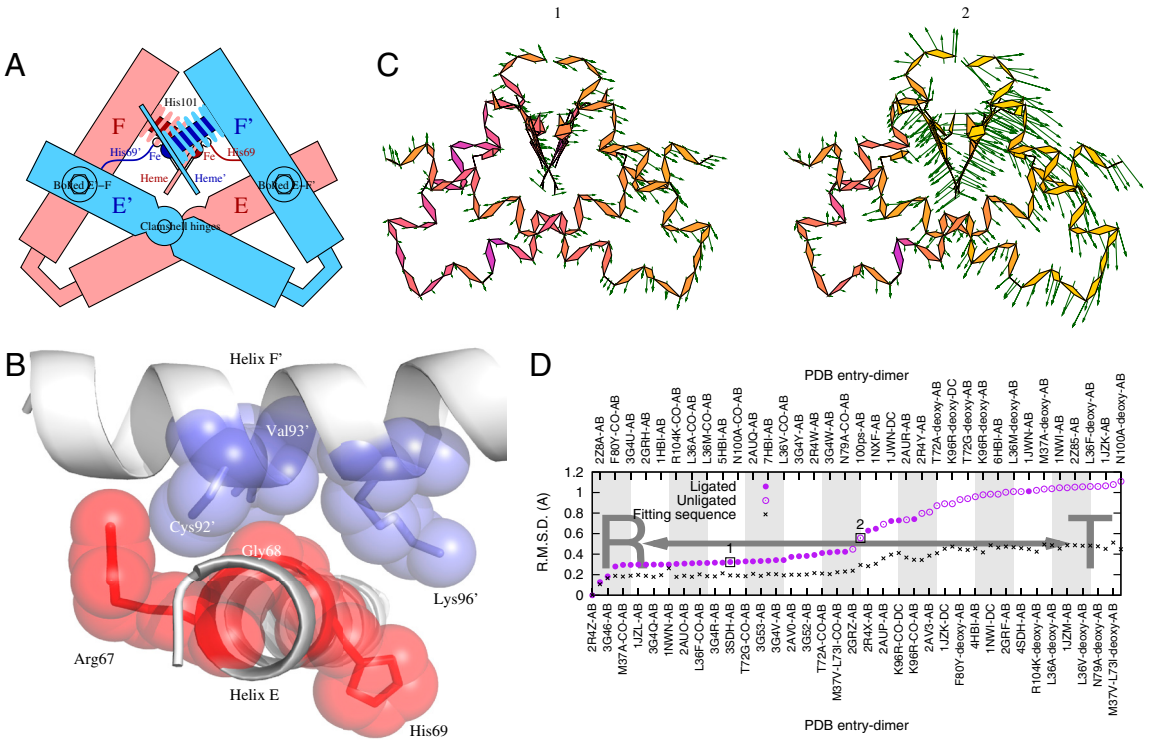

Fig. 1. A mechanical model of cooperative HbI homodimer. Subunits A and B in *A* and *B* are colored in red and blue, respectively. Only helices E and F are shown in *A* and *C*. (*A*) A schematic representation. See also Movie S1 for this mechanical device in action. (*B*) Key residues constituting intersubunit E–F′ contact. (*C*) Observed conformational changes in the same view as *A*. Two representative interfaces, numbered and outlined by black squares in *D*, are shown, with 1 corresponding to the wild-type HbI-CO (3SDH) and 2 corresponding to the 100-ps photoproduct reported here. Green arrows represent directions and amplitudes of atomic displacements from a reference structure 2R4Z with five times the lengths of actual displacements. See also Movies S2 and S3. (*D*) Structural similarity of dimer interface. All available dimeric structures of HbI (including the DC dimers in $P2_1$ space group) and the 100-ps refined structure are superimposed by least-squares fitting of a segment consisting of the end of helix E, the entire helix F of subunit A, and the beginning of helix E′ of subunit B. The alignment rmsd values are plotted using x symbols. Filled dots and open circles represent ligated and unligated states, respectively.

also been previously observed in myoglobin (9, 10) and human tetrameric hemoglobin (11). Principal component analysis (PCA) (12) also validates that the clamshell motion is the dominant motion (Fig. S2). All low-affinity, T-state HbI structures feature E–F spatial arrangement further apart from each other than those high-affinity R-state structures. We interpret that the high-affinity R state is likely achieved by closing E and F upon ligand binding. Conversely, the heme pocket opens upon ligand dissociation and results in a low-affinity T state. It is known that a ligated heme group drops deeper into its binding pocket via an in-plane motion (7), and an unligated heme is more exposed to the dimer interface. This heme motion, visible in Movie S3, seems to be driven by a component of the clamshell motion of F shown in Fig. 2*C* and maximized by the fact that the heme group is anchored to F near its end at the position F8. We further note that Lys96′ and Phe97′ from the partner subunit across the dimer interface cover the heme binding pocket in the ligated state and swing open in the unligated state (Fig. 3), which helps intersubunit communication of ligand binding states. One of these two residues Lys96′ directly involves intersubunit coupling via the bolt region (Fig. 1*B*). In conclusion, the clamshell motion of E and F correlates with the ligand-binding affinity. The size and tightness of a heme-binding pocket, the strategic location of the distal histidine next to the E–F′ junction, the in-plane sliding of the heme group with respect to the dimer interface, and the shielding provided by Lys96′ and Phe97′ from the partner subunit all contribute to structural modulation of ligand binding affinity in HbI.

(*ii*) Visual evidence shows that the hinge location for the E–F motion is near the middle of E rather than at the EF corner (Movie S2). We further design a crease-finding algorithm that determines the exact location of this clamshell hinge around Met74 at E12 position (Fig. S3). This specific hinge location ensures efficient motion transmission from one subunit to another: An increase in the E′–F′ angle in the blue subunit leads to an opening of the E–F angle in the red (Fig. 1*A*).

(*iii*) Fig. 4 shows quaternary rotation of the subunits (8) found in all HbI structures in PDB, sorted from very little rotation, with respect to the R state, to significant rotation of several degrees. Strikingly, motion of F′ in B is strictly associated with the entire A (Fig. 4), suggesting that F′ is tightly coupled with A instead of its own subunit, B. We therefore postulate that the quaternary rotation between A and B is powered by the motion of F′ with respect to the rest of B (Fig. 2). It is previously known and here confirmed by our PCA (Fig. S4) that this rotation is about an axis normal to the subunit interface and passes near the junction of the two E helices (8). As the E-to-E′ contact is very close to the rotation axis, only a small structural adjustment is required to accommodate the rotation, where rearrangement of an ordered water cluster has been found (13, 14). Meanwhile, both E-to-F′ and E′-to-F junctions, about 12 Å away from the quaternary rotation axis, remain intact so that motions of F in one subunit can be directly transmitted to E in the other subunit. We identify that a tight coupling at these junctions based on a dovetailed structure is responsible for efficient cross-interface motion transmission. This intersubunit coupling in HbI is formed by Arg67, Gly68, distal His69, Cys92′, Val93′, and Lys96′ (Fig. 1*B*), residues that are conserved among known arcid hemoglobins (15). Crystal structures of other invertebrate hemoglobins also exhibit similar EF dimers (1, 2) that utilize close contacts involving equivalent residues (Fig. S5). These additional examples suggest that such tight intersubunit coupling represent a common allosteric signaling mechanism among invertebrate hemoglobins despite their limited

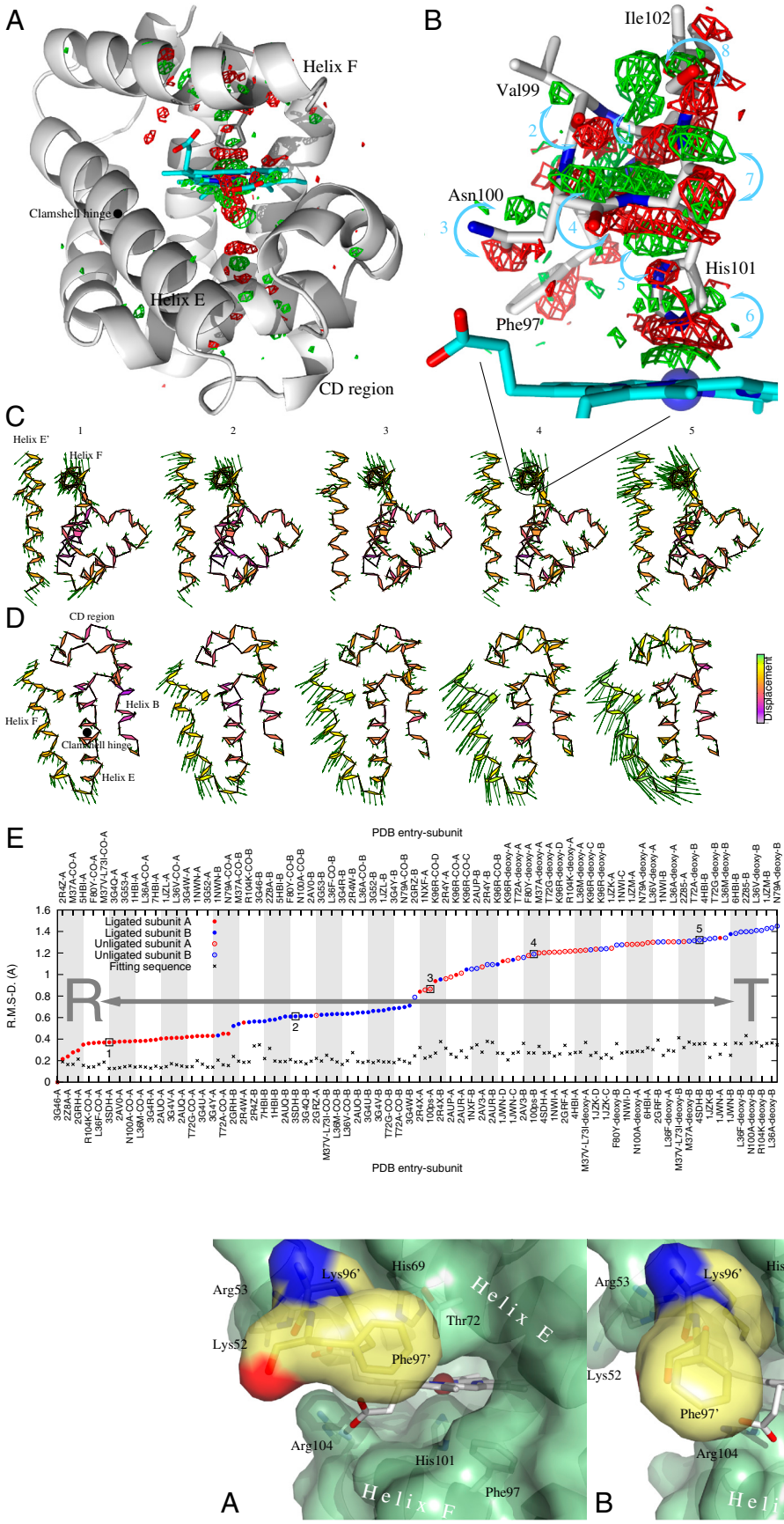

Fig. 2. Motion of helix F. (*A*) Difference map at 100 ps after CO photodissociation in subunit B. The difference map is calculated by Fourier synthesis of $F_{light} - F_{dark}$ with phases from the dark model (3SDH) at a resolution of 1.6 Å and contoured at $+7\sigma$ in green and -7σ in red. (*B*) Zoom-in view. The proximal part of the map in *A* is contoured at $\pm 5\sigma$. Part of helix F from Phe97 to Ile102 is shown in stick model in gray as viewed along the helix, similar to the perspective shown in *C*. Arrows in light blue mark pairs of positive and negative densities to aid the visualization of the helix F motion. (*C*) Motion of helices F and E′. For analyses in *C*, *D*, and *E*, both subunits A and B from all available structures of HbI and the 100-ps refined structure, including subunits D and C in $P2_1$ space group, a total of 140 subunits, are superimposed by least-squares fitting of helix B, CD region, and first half of helix E. The alignment rmsd values are plotted in *E* by x symbols and serve as an estimate of noise level. Five representative structures corresponding to the outlined data points in *E* are shown. The viewpoint is along helix F and with helix E′ nearly vertical. (*D*) Clamshell motion of helix F relative to E. The clamshell motion is parameterized by interhelix E-F distance and angle (Fig. S6). (*E*) Rmsd as a measure for structural similarity (5). Ligated and unligated subunits are represented by filled dots and open circles, respectively. Subunits A and B are colored in red and blue, respectively. Released PDB entries are marked by access code-subunit. Other structures (J.E.K. and W.E.R.) are labeled by mutation-ligation-subunit.

Fig. 3. Heme binding pocket in ligated (*A*) and unligated (*B*) states. Protein surface of one subunit is represented in light green. Heme group is shown in stick model. Helices E and F, and several key residues are labeled. Lys96′ and Phe97′ of the partner subunit function as a ligand controlled lid that shields the heme binding cavity. Residues from the partner subunit are shown in yellow surface with red and blue indicating O and N, respectively.

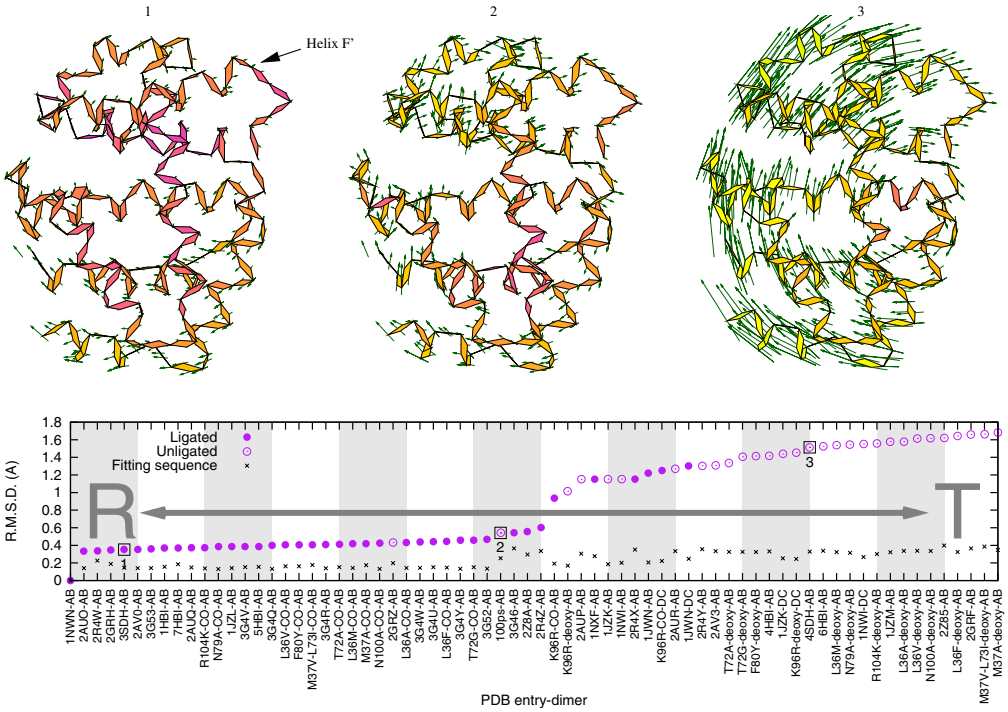

Fig. 4. Quaternary structural change. All available dimeric structures of HbI (including DC dimers in $P2_1$ space group) and the 100-ps refined structure are superimposed by least-squares fitting of helix B, CD region, and the first half of helix E of subunit B, revealing a rotation of subunit A relative to subunit B (8). AB dimer in 1NWN and DC dimer in 1NWI are identified as two extremes in the rotation range. Filled dots and open circles represent ligated and unligated states, respectively. The alignment rmsd values are plotted by x symbols. Three representative dimers are numbered and outlined by black squares and shown above the plot in the corresponding order from a perspective viewing into the dimer interface of subunit A. Only subunit A and helix F from subunit B, as labeled helix F′, are shown. The arrow length is amplified by three times the atomic displacement. The motion of F′ blends in that of subunit A completely as judged by false colors and arrows, indicating a concerted motion of F′ and subunit A.

sequence homology. A Gly residue without side chain or an Ala residue with the smallest side chain at the position E6 next to the distal His at E7 seems to be required for this purpose. We have also conducted normal mode analysis of various elastic network models (16) of HbI. We attribute the lack of good prediction of the observed motions resulting from these attempts to the incorrect representation of this tight, thus inelastic, intersubunit coupling by the elastic networks (*SI Text*).

(*iv*) To demonstrate how the proposed mechanical model operates halfway through the R-to-T transition, a structure is required in which a ligated subunit is homogeneously complexed with an unligated one. In the absence of a direct observation, we examine structural asymmetry between subunits related by NCS. Because both E–F distance and angle in ligated B are greater than those in ligated A (Fig. S6), E and F are separated further apart in B than in A in all ligated structures, as systematically shown in Fig. 2 *D* and *E*. Sorted by structural similarity in Fig. 2*E*, consecutive red dots suggest similarity among all structures of ligated A, while consecutive blue dots represent ligated B also structurally alike to one another but distinct from ligated A. However, the systematic distinction between A and B is found to be much weaker for the unligated state, as evident from the scrambled order of red (A) and blue (B) open circles in Fig. 2*E*. These T-state open circles show a gradual transition away from the R-state solid dots. Therefore, we conclude that in crystal lattices, a ligated B has a larger heme-binding pocket, thus lower ligand binding affinity, and is typically less R-like compared to a ligated A. As a result, a ligated B should release its ligand more readily than a ligated A does. This is supported by time-resolved crystallographic observations (14, 17) showing that B exhibits consistently greater photodissociation of CO than A does.

Time-resolved studies of *Scapharca* wild-type and mutant M37V HbI conducted with ns time resolution (14, 17) have demonstrated rapid formation of intermediate structures upon photodissociation of the CO ligand. Most tertiary conformation changes occur at and near the heme groups. We report here similar experiments on wild-type HbI with time resolution extending to 100 ps and further refine a structure against the 100-ps photoproduct dataset (Table S1). Compared to the initial CO-bound R state (3SDH), the 100-ps photoproduct exhibits a larger E–F angle in both subunits. Although asymmetry between subunits is present mostly in the ligated state, the dimer structure at 100 ps remains asymmetric. Sorted by the motion of F (Fig. 2*E*), B agrees well with the T-like unligated state, while A is situated at the beginning of the unligated range. The clear difference between A and B at 100 ps results from an asymmetric starting point before ligand dissociation—that is, ligated B being already further advanced toward the unligated T region than ligated A (Fig. 2*E*). Furthermore, the crystal packing environment appears to be more favorable for ligand dissociation in B. The quaternary rotation between the subunits has clearly already begun as early as 100 ps and just reached a point ready for a large transition to a fully unligated T state (Fig. 4). Fig. 1*C* and Movie S2 show that evidence (*iv*), the asymmetric motion, is indeed present in all known dimer structures of HbI as well as in the newly obtained 100-ps structure that depicts the mechanical model partially through the R-to-T transition.

Discussion

In summary, our model of cooperative action in HbI (Fig. 1*A* and Movie S1) illustrates a cascade of structural events that connect the initial triggering event of primary photodissociation to the final changes in ligand binding affinity of the secondary ligand, via tertiary conformational changes in various helices, quaternary rotation between the subunits, and motion transmission across the stable dimer interface. Within the context of *Scapharca inaequi-*

valvis HbI, we have shown that a change in ligation state is communicated between two heme sites via a delicate sequence of structural changes and that the quaternary rotation of a subunit between the T and R states is driven by the ligation state in its partner subunit via F, in which case distinction between tertiary and quaternary structural changes is extraneous. We construct an actual mechanical device (Movie S4) to demonstrate the proposed cooperative mechanism.

To put our proposed mechanical model in a broader context, we replicate figure 1 from ref. 5 in black (Fig. 5) to serve as an oversimplified summary of a dimeric allosteric system, and we add thick red arrows to show how these schematic models are related to the sequence of events in Movie S1. The primary photodissociation, more likely to occur in B in crystal lattices, takes place instantaneously prior to extensive structural response of the protein. At 100 ps, B has largely gone through the transition from R to T state judged by the structural feature of EF angle alone (Fig. 2). However, it would take longer for A to follow B and to complete the transition. The increased EF angle in A promotes the secondary, cooperative dissociation when it is forced to open. In addition, we also observe that B tends to be less R-like than A even in fully ligated state (Fig. 2), which suggests that the thin arrows in red might be a very minor pathway.

The essence of the Pauling–KNF allosteric model is that a singly ligated state features an asymmetric dimer. Our time-resolved structure at 100 ps provides an experimental observation of such asymmetric and partially ligated state located at the center of Fig. 5. On the other hand, the MWC allosteric model requires symmetric dimers in both ligated and unligated states. We provide a structural mechanism for the dimer to stay in symmetry. Any ligand event, which disturbs one of the subunits and thereby temporarily knocks the dimer out of symmetry, would signal to the partner subunit to promote the same ligand event. The inner workings of the protein enable the dimer to regain its symmetry quickly after any asymmetry occurs. As a result, all dimers stay symmetric on the physiological time scale regardless of their ligation state. Asymmetric dimers are present only transiently. Thus, in this system, the previous allosteric theories are unified.

This simple mechanical model not only provides a structural basis that satisfactorily explains the cooperative behavior of the HbI homodimer but also suggests a general mechanism for transmitting motions and signals across an interface between subunits or domains, in which effective signaling critically relies on a firm, stable interface without major disruption or structural rearrangements. A biological dimer or higher functional oligomer forms not merely to multiply the action of a monomer but more importantly to work cooperatively to carry out its function otherwise impossible as independent monomers. Scissors and pliers might be proper analogies, because they are both homodimeric and cooperative devices. It remains to be seen whether similar principles apply to other allosteric systems. Nevertheless, the meta-analysis of a large set of protein structures presented here may be a valuable tool to address functional motions in a wide variety of macromolecular systems.

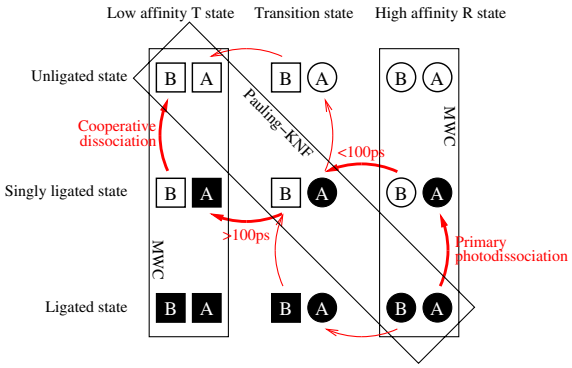

Fig. 5. Dimeric allosteric system. The black diagram is a reproduction from ref. 5. The low affinity T state is represented by two square symbols. The high affinity R state is in two circular symbols. The transition state is indicated by mixed symbols. Open and filled symbols stand for unligated and ligated states, respectively. The thick and thin arrows in red mark the major and possible minor pathways.

Methods

Time-Resolved Laue Diffraction Datasets. Time-resolved Laue diffraction datasets are collected at BioCARS 14-ID beamline at the Advanced Photon Source, Argonne National Laboratory. See refs. 13 and 15 for the time-resolved data collection protocol and parameters. Diffraction images are processed by the software package *Precognition*™ (Renz Research, Inc.). The 100-ps structure of the HbI-CO photoproduct is refined by a real space protocol against a weighted (18) difference electron density map (Fig. 2 *A* and *B*) between a 100-ps photoproduct and a dark, reference dataset of HbI-CO (Table S1).

Alignment and Displacement rmsd. Conformational change and structural motion revealed by comparison of two or more structures require least-squares fitting in three-dimensional space. It is common that an overall rmsd value of the fitting is chosen as an indicator for the amplitude of change or motion. We suggest distinguishing two structural segments from each other: One segment is used for alignment using least-squares fitting, another segment for evaluation of conformational change or motion. These two segments may be the same, partially overlap, or entirely different as a specific comparison requires. The rmsd values of these two segments are therefore denoted as rmsd of alignment and displacement, respectively. The alignment rmsd indicates how well the alignment segments fit together. The displacement rmsd quantifies the amplitude of structural change. The difference or ratio between these two rmsd values indicates the significance of a specific structural change with respect to other structural variations.

Differentiation of Structures Related by Noncrystallographic Symmetry. Solution-based techniques probing an ensemble of structures cannot distinguish between chemically identical subunits. In contrast, arbitrarily assigned A/B subunits of HbI related by NCS are packed in distinct environments in a crystal lattice (Fig. S1). Their environmental differences are systematically repeated 10^{12} times across an entire crystal and are experimentally recorded by X-ray diffraction. Such differences are traditionally considered crystallization artifacts and thus are often dismissed. Previous works (14, 17) and further structural analysis presented in this work (Fig. 2*E* and Figs. S6 and S7) clearly show that the crystal lattice accommodates a dimer in which the two subunits represent distinct yet functionally important conformations. Our underlying strategy is to treat molecular packing environments in crystal lattices derived from NCS and crystallization conditions as a unique probe of dynamic behaviors of proteins. As a consequence of such distinct environments, static and dynamic differences between crystal structures related by NCS are informative, independent measurements (6, 19).

Joint Analysis of Related Crystal Structures. Joint analysis of related crystal structures derived from different sources, including space groups, crystallization conditions, ligation states, different complexes, mutants, and even different species, can reveal more structural insights, which is otherwise inaccessible by individual inspection of static structures and small scale structural comparison. This strategy is similar to the principle of meta-analysis, a common analytical approach used in biomedical and clinical research. Compared to the vast, multidimensional conformation space of a protein in solution, accessible conformation subspace is rather limited in a crystal lattice under a given crystallization condition. Meta-analysis of a collection of related structures derived from a variety of sources, as demonstrated in this study, provides a much broader survey of the conformation space and thereby has the potential to unravel dynamical characteristics of a protein structure and its functional pathway.

ACKNOWLEDGMENTS. We thank W. Y. Chan, X. Yang and K. Moffat for critical discussions and reading of the manuscript. We thank J. Andrew for editorial assistance. Use of the Advanced Photon Source was supported by the US Department of Energy, Basic Energy Sciences, Office of Science, under Contract DE-AC02-06CH11357. Use of the BioCARS Sector 14 was supported by the National Institutes of Health (NIH), National Center for Research Resources, under Grant RR007707. The time-resolved setup at Sector 14 was funded in part through collaboration with P. Anfinrud (NIH/National Institute of Diabetes and Digestive and Kidney Diseases).

1. Royer WE, Knapp JE, Strand K, Heaslet HA (2001) Cooperative hemoglobins: Conserved fold, diverse quaternary assemblies and allosteric mechanisms. *Trends Biochem Sci* 26:297–304.
2. Royer WE, Zhu H, Gorr TA, Flores JF, Knapp JE (2005) Allosteric hemoglobin assembly: Diversity and similarity. *J Biol Chem* 280:27477–27480.
3. Eaton WA, Henry ER, Hofrichter J, Mozzarelli A (1999) Is cooperative oxygen binding by hemoglobin really understood? *Nat Struct Mol Biol* 6:351–358.
4. Eaton WA, et al. (2007) Evolution of allosteric models for hemoglobin. *IUBMB Life* 59:586–599.
5. Cui Q, Karplus M (2008) Allostery and cooperativity revisited. *Protein Sci* 17:1295–1307.
6. Kondrashov DA, Zhang W, Aranda R, Stec B, Phillips GN (2007) Sampling of the native conformational ensemble of myoglobin via structures in different crystalline environments. *Proteins* 70:353–362.
7. Royer WE (1994) High-resolution crystallographic analysis of a cooperative dimeric hemoglobin. *J Mol Biol* 235:657–681.
8. Knapp JE, Royer WE (2003) Ligand-linked structural transitions in crystals of a cooperative dimeric hemoglobin. *Biochemistry* 42:4640–4647.
9. Kachalova GS, Popov AN, Bartunik HD (1999) A steric mechanism for inhibition of CO binding to heme proteins. *Science* 284:473–476.
10. Cammarata M, et al. (2008) Tracking the structural dynamics of proteins in solution using time-resolved wide-angle X-ray scattering. *Nat Methods* 5:881–886.
11. Kneipp J, et al. (2006) Dynamics of allostery in hemoglobin: Roles of the penultimate tyrosine H bonds. *J Mol Biol* 356:335–353.
12. Yang L-W, Eyal E, Bahar I, Kitao A (2009) Principal component analysis of native ensembles of biomolecular structures (PCA_NEST): Insights into functional dynamics. *Bioinformatics* 25:606–614.
13. Royer WE, Pardanani A, Gibson QH, Peterson ES, Friedman JM (1996) Ordered water molecules as key allosteric mediators in a cooperative dimeric hemoglobin. *Proc Natl Acad Sci USA* 93:14526–14531.
14. Knapp JE, Pahl R, Šrajer V, Royer WE (2006) Allosteric action in real time: Time-resolved crystallographic studies of a cooperative dimeric hemoglobin. *Proc Natl Acad Sci USA* 103:7649–7654.
15. Royer WE (1992) Structures of red blood cell hemoglobins. *Advan Comp Environ Physiol* 13:87–116.
16. Tirion MM (1996) Large amplitude elastic motions in proteins from a single-parameter, atomic analysis. *Phys Rev Lett* 77:1905–1908.
17. Knapp JE, et al. (2009) Ligand migration and cavities within *Scapharca* dimeric HbI: Studies by time-resolved crystallography, Xe binding, and computational analysis. *Structure* 17:1494–1504.
18. Ren Z, et al. (2001) A molecular movie at 1.8 A resolution displays the photocycle of photoactive yellow protein, a eubacterial blue-light receptor, from nanoseconds to seconds. *Biochemistry* 40:13788–13801.
19. Kovaleva EG, Lipscomb JD (2007) Crystal Structures of Fe^{2+} dioxygenase superoxo, alkylperoxo, and bound product intermediates. *Science* 316:453–457.